(Received 14 April 2024, Accepted 27 May 2024, Scheduled 6 June 2024)

Broadband Generation Orbital Angular Momentum Beams Based on Uniform Phase Error Analysis of Uniform Circular Array

Na Li[1,*], Lingling Jiao[2], Guirong Feng[3], Ping Li[4], and Xiaowei Shi[4]

[1]*Shool of Electronic Engineering, Xidian University, Xi'an 710071, China*
[2]*Academy of Advanced Interdisciplinary Research, Xidian University, Xi'an 710061, China*
[3]*Shool of Electronic Engineering, Xi'an University of Posts and Telecommunications, Xi'an 710071, China*
[4]*National Key Laboratory of Antennas and Microwave Technology, Xidian University, Xi'an 710071, China*

ABSTRACT: In this paper, we propose a method for generating broadband orbital angular momentum (OAM) beams utilizing the two neighboring ports of the uniform circular array (UCA) excited with a phase difference of $(2(\pi+\delta)l)/N$. This approach differs from current arrays used to generate an OAM beam with a phase difference of $2\pi l/N$. We establish that the UCA can produce OAM beams covering 83% (7-17 GHz) of the bandwidth. The array antenna consists of three Vivaldi elements with a phase difference between adjacent ports, capable of generating OAM beams of mode 2 when being fed with equal amplitude and phase. In contrast to current OAM antenna arrays that require complex phase-shifting networks for feeding, our proposed antenna array offers simplicity in its feeding mechanism. Furthermore, the UCA-based Vivaldi antenna presents a novel approach for generating wideband OAM beams and holds significant potential for applications in broadband communication.

1. INTRODUCTION

Because of the orthogonality of integer topological modes and the benefits of rotational degrees of freedom, orbital angular momentum (OAM) technology provides distinct advantages in the fields of 6G mobile communication [1] and radar imaging [2]. OAM beam-based multiplexing technology has the potential to greatly increase the capacity of transmission [3–5]. High-speed data transmission using ultra-wideband (UWB) technology has benefits such as low power consumption, little interference, cost-effectiveness, and security [6]. Combining the advantages of UWB technology and the strong anti-interference ability of OAM beam, it is expected to greatly improve the performance of communication system. However, the OAM communication systems described in [7–9] are all narrowband systems, which are difficult to meet the stability and efficiency requirements of modern communication systems. In addition, as a widely accepted OAM communication system, the future ultra-high data rate backhaul transmission will undoubtedly require large bandwidth. In the field of radar imaging, the feasibility of OAM based radar imaging has been demonstrated in a variety of mechanisms [10–13]. But most published systems are built for single-frequency or narrowband OAM beams, with an emphasis on azimuth super-resolution imaging [11–13]. To attain great range resolution, vortex beams carrying OAM must have a large bandwidth [14, 15]. Consequently, it is crucial to produce OAM beams in the broadband range.

Since the first experimental demonstration of radio frequency waves was announced in 2007, a number of methods have been proposed for producing OAM beams. These techniques include microstrip patch antennas, helical antennas [16], reflectarrays [17], traveling-wave antennas [18], circular leaky-wave antennas [19], circular antenna arrays [20, 21], metasurfaces [22], spiral reflector plates [23], and twisted parabolic reflectors [24]. Sadly, because of their resonance characteristics, a large number of these OAM generators are limited to operating in a narrow frequency range. As an illustration, the bandwidths of the antennas mentioned in [17, 21] that can produce OAM are less than 0.06% and 0.1%, respectively.

In this paper, we propose a wideband OAM beam-generating antenna array. The antenna array consists of three Vivaldi elements. Specifically, the ports of neighboring Vivaldi antenna elements exhibit a phase difference of $(2(\pi+\delta)l)/N$. Therefore, when being fed with identical amplitude and phase, the antenna can generate OAM beams with mode $+2$ over a bandwidth of 83.3% (7–17 GHz). In contrast to current OAM antenna arrays that require complex phase-shifting networks for feeding, our proposed antenna array can generate broadband OAM beams without complex phase-shifting networks, thus reducing the system complexity. This paper provides a new method for wideband OAM beam generation.

* Corresponding author: Na Li (lina_xidian@stu.xidian.edu.cn).

2. OAM ANTENNA ARRAY DESIGN

2.1. Theoretical Analysis

OAM beams can be generated when the circular array elements are fed with identical amplitude but with phase difference $2\pi l/N$ between two adjacent elements. Referring to Figure 1, N array elements are evenly distributed around the circle. n is the nth element; P represents any point in the far-field space; and r denotes the distance between point P and the center of the array antenna. Each antenna element is fed with the equal amplitude and phase of $\beta_0 + n \cdot 2\pi l/N$, where β_0 is the beginning phase, and l is the topological charge. The azimuthal angle of the antenna element is $\varphi_n = 2\pi(n-1)/N$.

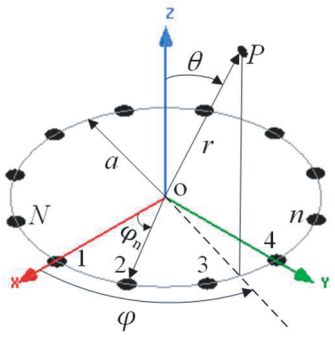

FIGURE 1. The schematic diagram of UCA.

According to the superposition principle of electromagnetic field, the electric field vector for point $P(\vec{r},\vec{\varphi},\vec{\theta})$ can be expressed as [25]

$$\begin{aligned} E &\approx \sum_n^N \frac{e^{-jk(r-a\cdot\sin\theta\cos(\varphi-\varphi_n))}}{r}\cdot e^{-j(\beta_0+n\cdot 2\pi l/N)} \\ &= \frac{e^{-jkr}}{r}\sum_n^N\sum_{m=-\infty}^{+\infty} j^m J_m(ka\sin\theta)e^{jm(\varphi-n\cdot 2\pi/N)} \\ &\quad \cdot e^{j(\beta_0+n\cdot 2\pi l/N)} \\ &= N\cdot\frac{e^{-j(kr-\beta_0)}}{r}\cdot\sum_\mu j^{l-\mu N}J_{l-\mu N}(\beta)\cdot e^{j(l-\mu N)\varphi}, \\ &\quad (\mu = 0,\pm1,\pm2\ldots) \end{aligned} \tag{1}$$

where $j=\sqrt{-1}$ is the imaginary unit, k the wave vector, and $J_{1-uN}(\cdot)$ is $(1-uN)$th-order Bessel function of the first kind. Considering $\mu = 0$, and $J_{1-uN}(\beta)$ will get the maximum. Then, Eq. (1) can be written as

$$E = \frac{e^{-j(kr-\beta_0)}}{r}\cdot\sum_\mu j^l J_l(\beta)\cdot e^{jl\varphi} \tag{2}$$

It can be seen from Eq. (2) that the array can generate vortex wave mode l, when the feeding phase of the n-th element $\beta_n{=}\beta_0{+}n{\cdot}\Delta\varphi$, where $\Delta\varphi = 2\pi l/N$.

When the phase difference between the elements has a uniform error, $\Delta\varphi$ changes $(2\pi+\delta)l/N$. Then, the feeding phase of the n-th element is $\beta_n{=}\beta_0{+}(n\%(\frac{N}{l}))\cdot\Delta\varphi$, and the electric field vector can be expressed as

$$\begin{aligned} E &\approx \frac{e^{-jkr}}{r}\sum_{n=0}^{N-1}\sum_{m=-\infty}^{+\infty} j^m J(ka\sin\theta)e^{jm(\varphi-n\cdot 2\pi/N)} \\ &\quad \cdot e^{j(\beta_n)} \\ &= \frac{e^{-j(kr-\beta_0)}}{r}\sum_{m=-\infty}^{+\infty} j^m J_m(\beta)e^{jm\varphi}\sum_{g=0}^{l-1} e^{-jm\frac{2\pi}{l}\cdot g} \\ &\quad \sum_{n=0}^{N/l-1} e^{j\left(1-\frac{m}{l}+\frac{\delta}{2\pi}\right)\cdot\frac{2\pi}{N/l}\cdot n} \end{aligned} \tag{3}$$

Because we know

$$\sum_{g=0}^{l-1} e^{-j(m)\cdot\frac{2\pi}{l}\cdot n} = \begin{cases} l & m=\mu_1 l \\ 0 & m=\mu_1 l \end{cases} \qquad \mu_1 = \pm1,\pm2\ldots$$

Eq. (3) can be written as

$$\begin{aligned} E &\approx l\cdot\frac{e^{-j(kr-\beta_0)}}{r}\sum_{\mu_1} j^{(\mu_1 l)}J_{\mu_1 l}(\beta)e^{j(\mu_1 l)\varphi} \\ &\quad \sum_{n=0}^{N/l-1} e^{j((1+\frac{\delta}{2\pi}-\mu_1))\frac{2\pi}{N/l}\cdot n} \\ &\quad \sum_{n=0}^{N/l-1} e^{j((1+\frac{\delta}{2\pi}-\mu_1))\frac{2\pi}{N/l}\cdot n} \end{aligned} \tag{4}$$

In Eq. (4), we know

$$\sum_{n=0}^{N/l-1} e^{j((1+\frac{\delta}{2\pi}-\mu_1))\frac{2\pi}{N/l}\cdot n} = \frac{e^{j(\delta)}-1}{e^{j(\delta)\cdot\frac{l}{N}}-1} \tag{5}$$

when δ is minimum, $e^{j\delta l/N}\approx 1+\delta l/N$. Eq. (4) can be written as

$$\begin{aligned} E &\approx l\cdot\frac{e^{-j(kr-\beta_0)}}{r}\sum_{\mu_1} j^{(\mu_1 l)}J_{\mu_1 l}(\beta)e^{j(\mu_1 l)\varphi}\cdot(e^{j(\delta)}-1)\cdot\frac{N}{l\cdot\delta} \\ &= \frac{N}{\delta}\frac{e^{-j(kr-\beta_0)}\cdot(e^{j(\delta)}-1)}{r}\sum_{\mu_1} j^{(\mu_1 l)}J_{\mu_1 l}(\beta)e^{j(\mu_1 l)\varphi} \end{aligned} \tag{6}$$

It can be seen from Eq. (6) that the array can generate vortex wave mode $\mu_1 l$, when the feeding phase of the nth element is $\beta_n{=}\beta_0{+}(n\%(N/l))\cdot(2\pi+\delta)l/N$. When $\mu_1 = 1$, $J_{\mu_1 l}(\beta)$ will get the maximum. So, the array can also produce the OAM mode l with uniform phase errors.

2.2. Electromagnetic Simulations

To validate the feeding form of the UCA and the formula derivation mentioned above, we developed a UCA model. The model was designed and simulated using ANSYS Electronics full-wave simulator, as depicted in Figure 2. The UCA consists of $N{=}$ 6 monopole antennas designed at 6 GHz, with a radius of 11 mm. The P1–P6 ports were fed with same amplitude I and phase β_n $(\beta_0{+}(n\%(\frac{N}{l}))\cdot\Delta\varphi)$. The phase fronts of the electric fields (E_Z) at various phase errors (δ) in observation

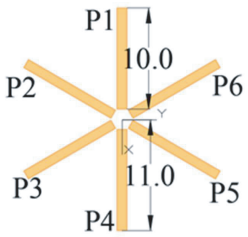

FIGURE 2. The UCA model.

plane are indicated in Table 1. The observation plane's dimensions are $2\lambda \times 2\lambda$, and the distance between it and the UCA is λ.

Table 1 demonstrates that the two spiral arms are clearly visible under different δ, and the phase distribution shows a change of $2\pi \cdot 2$ along the azimuth. The calculation of mode purity reveals a gradual decrease with an increase of δ, but it remains greater than 50%. As thus, the array can produce the OAM modes of 2. Therefore, when the array's phase is $\beta_0 + (n\%(N/l)) \cdot \Delta\varphi$, and amplitude is identical, an OAM beam with mode l can also be produced. However, as the phase error δ rises, the purity rapidly decreases, as can be seen from the purity computation.

TABLE 1. The phase distributions at different δ.

δ	The phase of the ports	The phase fronts of E_Z	The mode purity of E_Z
0	P1 0° P2 120° P3 240° P4 0° P5 120° P6 240°	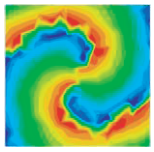	69.4%
-π/4	P1 0° P2 105° P3 210° P4 0° P5 105° P6 210°	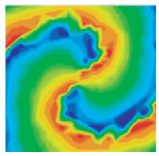	64.1%
-π/3	P1 0° P2 100° P3 200° P4 0° P5 100° P6 200°	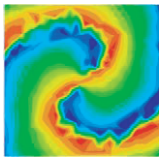	62.4%
-π/2	P1 0° P2 90° P3 180° P4 0° P5 90° P6 180°	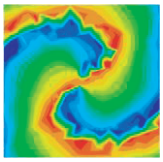	59.3%
-2π/3	P1 0° P2 80° P3 160° P4 0° P5 80° P6 160°	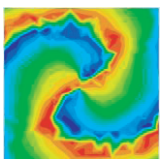	56.6%

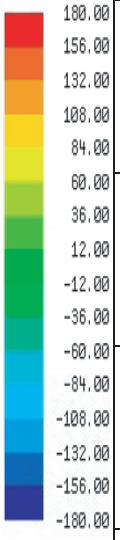

3. BROADBAND OAM GENERATION ANTENNA ARRAY

3.1. Antenna Array Design

The circular array is produced in Figure 3 by combining three UWB Vivaldi antennas. The array antenna has a mortise and tenon structure, dividing the azimuth plane into six equal pieces with a radius of $R = 0.56\lambda c$, which is the array's operational wavelength at the center frequency. A double-slot structure was initially proposed for the original Vivaldi antenna to prevent beam splitting and increase gain in high frequency bands [26]. In the study, the double-slot Vivaldi antenna element of the OAM array is designed as two nearly symmetric components, each with three layers. Their substrates are Rogers5880, which have a relative permittivity of 2.2 and a thickness of 0.254 mm. Table 2 displays the structural parameters.

The ports are fed with equal amplitude but have a phase difference of $2\pi l/N$ in impedance bandwidth, a UWB OAM beam is formed. The Vivaldi antenna elements were fed with stripline-slotline transitions of different lengths, and the length difference between two adjacent Vivaldi antenna elements was

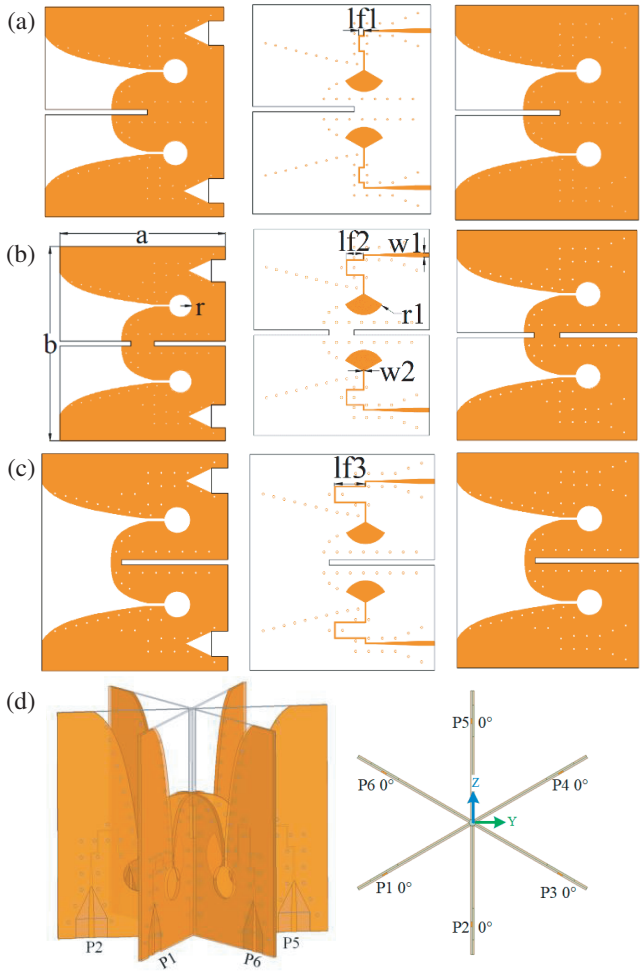

FIGURE 3. The Vivaldi antenna. (a) element 1; (b) element 2; (c) element 3; from left to right are the upper layer, middle layer and bottom layer. (d) the antenna array, from left to right are the side view and the back view.

TABLE 2. Structural parameters of the Vivaldi antenna element.

Parameters	Value (mm)	Parameters	Value (mm)
a	41	$lf1$	1
b	35	$lf2$	3.5
r	2.5	$lf3$	6
$w1$	0.8	$w2$	0.2

optimized. Subsequently, a corresponding phase difference exists between adjacent Vivaldi antenna elements, and this phase difference varies at different frequencies. So, the Vivaldi antenna can produce UWB OAM beams by setting the various phase differences in Table 1 at different frequency locations. The stripline-slotline transitions of the Vivaldi antenna elements shown in Figure 3 are at different lengths ($lf1, lf2, lf3$). We performed a simulation analysis for the different stripline-slotline transitions using the same lengths in Figure 4. Figure 5 shows the phase difference of the ports in Figure 4. The phase discrepancies between the ports at 12 GHz are 240° and 120°, respectively, so there is a 120° phase difference between ports P1 and P6 of the antenna array and a 240° phase difference between ports P2 and P1. It can be concluded that the feeding phase is consistent with $\delta = 0$ in Table 1. That is, at 12 GHz, the antenna array can generate OAM beams of mode 2. At 8 GHz, the phase difference between antenna array ports P2 and P1 is $-80°$, and the phase difference between ports P1 and P6 is $-160°$. The feed phase corresponds to $\delta = -2\pi/3$ in Table 1. Therefore, the antenna array can also produce OAM beams with mode 2 at 8 GHz. According to Figure 5, the phase of ports at different frequencies can be equivalent to $(n\%(6/2))\cdot(2\pi + \delta) \cdot 2/6$, so it enables the antenna array to emit OAM beams with mode 2 over a bandwidth of 83.3% (7–17 GHz). The far-field radiation patterns at several frequencies between 7 and 17 GHz are shown in Figure 6. With reference to the coordinate system shown in Figure 3, it is evident that all radiation zeros point in the direction of $-x$, suggesting the existence of vortex waves.

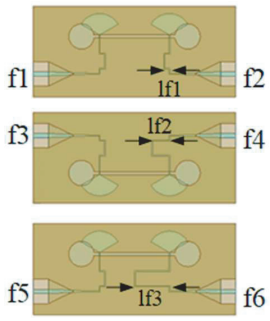

FIGURE 4. The model of the stripline-slotline transition.

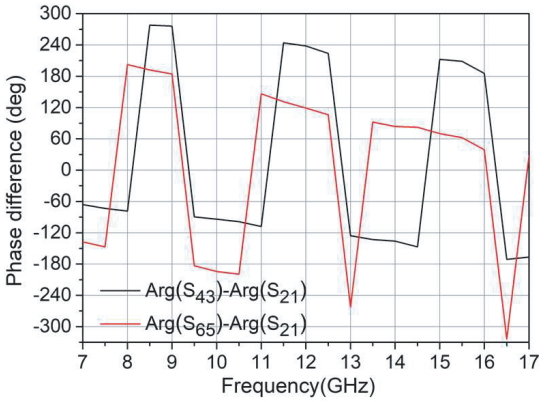

FIGURE 5. The phase difference of the ports.

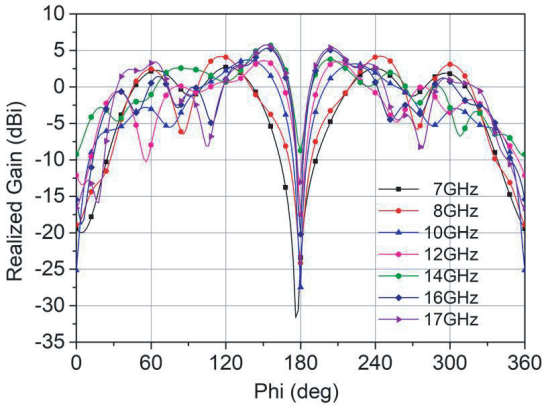

FIGURE 6. Simulated array far-field directional patterns.

3.2. Results and Discussions

In order to further prove the rationality of this method, the antenna array is fabricated as shown in Figure 7. The antenna array measurement results are shown in Figure 8 and Figure 9. The reflection coefficients of all the ports are less than -10 dB during 7–17 GHz, and the insertion loss between port 1 and the remaining five ports is displayed in Figure 9. It can be seen that for the working bandwidth of 7–17 GHz, the insertion loss is less than -20 dB, so the coupling between different ports is low. The antenna array fed with power divider is measured in a microwave anechoic chamber. The receiving probe is used to scan the E-fields of antenna at a distance of 2λ away, and the E_z phase distributions can be obtained on the observation with the size of $2\lambda \times 2\lambda$. Simulated and measured E_z phase

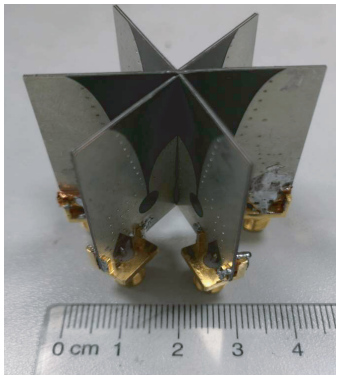

FIGURE 7. The photo of the Vivaldi array.

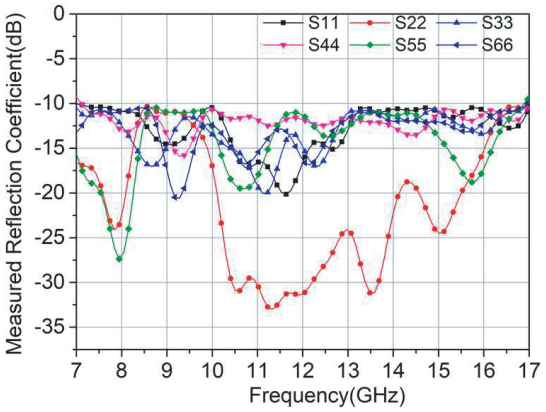

FIGURE 8. Measured reflection coefficient of the Vivaldi antenna ports.

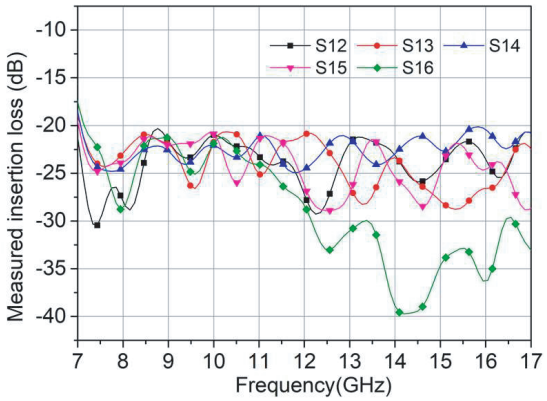

FIGURE 9. Measured insertion loss of the antenna ports.

TABLE 3. The simulated and measured of phase distributions.

Freq (GHz)	Simulated Mode +2 of E_Z	Measured Mode +2 of E_Z	The mode purity of E_Z
7	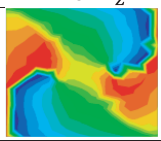	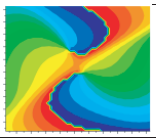	51.2%
10	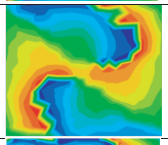	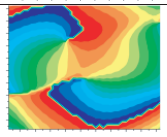	50.8%
12	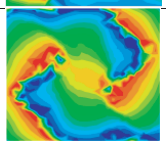	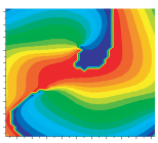	54.1%
14	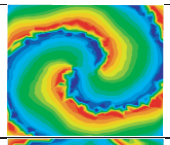	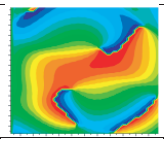	44.5%
17	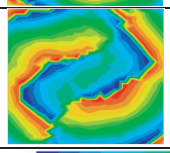 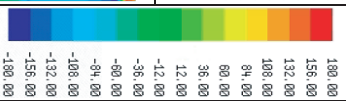	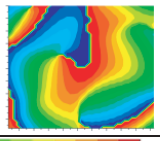	39.8%

distributions are shown in Table 3. Table 3 illustrates that two spiral arms are visible on the observation surface at different frequencies, and the phase exhibits a $2\pi \cdot 2$ change along the azimuth. The simulated phase distribution closely resembles the measured one. The calculation of modal purity indicates that the measured mode purity is lower than that of Table 1. This is mainly due to the phase error of the fed power divider, which reduces the purity of the OAM beam. As the fabricated antennas can generate the vortex beams over a bandwidth of 83.3% (7–17 GHz), the method and device proposed are practical and effective.

TABLE 4. Comparison of different OAM Vivaldi antenna array designs.

Reference	Bandwidth	Feed Network	Aperture
[28]	6–18 GHz	No	$2\lambda_c$
[29]	2.7–2.9 GHz	complex	$0.51\lambda_c$
[30]	6 GHz	No	$0.8\lambda_c$
Our work	7–17 GHz	simple	$0.56\lambda_c$

Compared to prior research employing Vivaldi antenna to generate vortex beams, as stated in Table 4, our work has more theoretical advancements, including creating the generation model for both element and array, as well as phase errors analysis. Furthermore, the antenna array can produce OAM without the requirement for complicated phase-shifting networks [27].

4. CONCLUSION

The UCA formula for generating OAM beams is derived, and a proposed excitation mechanism of UCA with phase errors for generating OAM beams is presented. It has been demonstrated that OAM beams can be generated when the phase of each array port is $(n\%(N/l)) \cdot (2\pi+\delta)l/N$. The efficiency of this approach is illustrated by mode purity calculations at different phase differences of error. The suggested antenna array consists of three Vivaldi antennas, which is based on the previously discussed theory and model. This array can produce OAM mode $+2$ over a bandwidth of 83.3% (7–17 GHz). Additionally, the array can create OAM beams using a power division network, which reduces system complexity and has applications in broadband communication combined with OAM systems. The excitation mechanism of the UCA holds significance for the broadband generation of OAM beams in practical applications.

REFERENCES

[1] Thidé, B., H. Then, J. Sjöholm, K. Palmer, J. Bergman, T. D. Carozzi, Y. N. Istomin, N. H. Ibragimov, and R. Khamitova, "Utilization of photon orbital angular momentum in the low-frequency radio domain," *Physical Review Letters*, Vol. 99,

No. 8, 087701, 2007.

[2] Zhang, Z., S. Xiao, Y. Li, and B.-Z. Wang, "A circularly polarized multimode patch antenna for the generation of multiple orbital angular momentum modes," *IEEE Antennas and Wireless Propagation Letters*, Vol. 16, 521–524, 2016.

[3] Yan, Y., G. Xie, M. P. J. Lavery, H. Huang, N. Ahmed, C. Bao, Y. Ren, Y. Cao, L. Li, Z. Zhao, and e. al., "High-capacity millimetre-wave communications with orbital angular momentum multiplexing," *Nature Communications*, Vol. 5, No. 1, 4876, Sep. 2014.

[4] Allen, B., A. Tennant, Q. Bai, and E. Chatziantoniou, "Wireless data encoding and decoding using OAM modes," *Electronics Letters*, Vol. 50, No. 3, 232–233, Jan. 2014.

[5] Wang, J., C. Cai, F. Cui, M. Yang, Y. Liang, and J. Wang, "Tailoring light on three-dimensional photonic chips: A platform for versatile OAM mode optical interconnects," *Advanced Photonics*, Vol. 5, No. 3, 036004, 2023.

[6] Lee, D., G. Shaker, and W. Melek, "A broadband wrapped bowtie antenna for UWB pulsed radar applications," *IEEE Transactions on Antennas and Propagation*, Vol. 68, No. 12, 7803–7812, Dec. 2020.

[7] Chen, R., H. Xu, M. Moretti, and J. Li, "Beam steering for the misalignment in UCA-based OAM communication systems," *IEEE Wireless Communications Letters*, Vol. 7, No. 4, 582–585, 2018.

[8] Zhang, Y., W. Feng, and N. Ge, "On the restriction of utilizing orbital angular momentum in radio communications," in *2013 8th International Conference on Communications and Networking in China (CHINACOM)*, 271–275, 2013.

[9] Xie, G., L. Li, Y. Ren, H. Huang, Y. Yan, N. Ahmed, Z. Zhao, M. P. J. Lavery, N. Ashrafi, S. Ashrafi, R. Bock, M. Tur, A. F. Molisch, and A. E. Willner, "Performance metrics and design considerations for a free-space optical orbital-angular-momentum-multiplexed communication link," *Optica*, Vol. 2, No. 4, 357–365, 2015.

[10] Zhang, Y., W. Feng, and N. Ge, "On the restriction of utilizing orbital angular momentum in radio communications," in *2013 8th International Conference on Communications and Networking in China (CHINACOM)*, 271–275, 2013.

[11] Yuan, T., H. Wang, Y. Cheng, and Y. Qin, "Electromagnetic vortex-based radar imaging using a single receiving antenna: Theory and experimental results," *Sensors*, Vol. 17, No. 3, 630, 2017.

[12] Wang, J., K. Liu, Y. Cheng, and H. Wang, "Three-dimensional target imaging based on vortex stripmap SAR," *IEEE Sensors Journal*, Vol. 19, No. 4, 1338–1345, 2019.

[13] Liu, K., Y. Cheng, Y. Gao, X. Li, Y. Qin, and H. Wang, "Superresolution radar imaging based on experimental OAM beams," *Applied Physics Letters*, Vol. 110, No. 16, 164102, Apr. 2017.

[14] Bamler, R., "Principles of synthetic aperture radar," *Surveys in Geophysics*, Vol. 21, No. 2, 147–157, 2000.

[15] Pan, S., X. Ye, Y. Zhang, and F. Zhang, "Microwave photonic array radars," *IEEE Journal of Microwaves*, Vol. 1, No. 1, 176–190, Jan. 2021.

[16] Yang, Y., K. Guo, F. Shen, Y. Gong, and Z. Guo, "Generating multiple OAM based on a nested dual-arm spiral antenna," *IEEE Access*, Vol. 7, 138 541–138 547, 2019.

[17] Beccaria, M., G. Dassano, and P. Pirinoli, "Single-layer, multimode OAM reflectarray antennas," *IEEE Antennas and Wireless Propagation Letters*, Vol. 22, No. 5, 980–984, May 2023.

[18] Zheng, S., X. Hui, X. Jin, H. Chi, and X. Zhang, "Transmission characteristics of a twisted radio wave based on circular traveling-wave antenna," *IEEE Transactions on Antennas and Propagation*, Vol. 63, No. 4, 1530–1536, Apr. 2015.

[19] Zhang, Q., W. Chen, H. Sun, J. Fu, Y. Zhao, H. Feng, and K. Zhang, "A circular-polarized vortex beams generation with orbital angular momentum based on a leaky-wave antenna," *IEEE Antennas and Wireless Propagation Letters*, Vol. 22, No. 6, 1311–1315, Feb. 2023.

[20] Zhang, Y.-M. and J.-L. Li, "Analyses and full-duplex applications of circularly polarized OAM arrays using sequentially rotated configuration," *IEEE Transactions on Antennas and Propagation*, Vol. 66, No. 12, 7010–7020, Dec. 2018.

[21] Zhang, Y.-M. and J.-L. Li, "Comments on "radial uniform circular antenna array for dual-mode oam communication"," *IEEE Antennas and Wireless Propagation Letters*, Vol. 17, No. 4, 719–721, Apr. 2018.

[22] Bai, H., G.-M. Wang, and T. Wu, "High-gain wideband metasurface antenna with low profile," *IEEE Access*, Vol. 7, 177 266–177 273, 2019.

[23] Stegenburgs, E., A. Bertoncini, A. Trichili, M. S. Alias, T. K. Ng, M.-S. Alouini, C. Liberale, and B. S. Ooi, "Near-infrared OAM communication using 3D-printed microscale spiral phase plates," *IEEE Communications Magazine*, Vol. 57, No. 8, 65–69, Aug. 2019.

[24] Spinello, F., G. Parisi, F. Tamburini, G. Massaro, C. G. Someda, M. Oldoni, R. A. Ravanelli, F. Romanato, and E. Mari, "High-order vortex beams generation in the radio-frequency domain," *IEEE Antennas and Wireless Propagation Letters*, Vol. 15, 889–892, Sep. 2015.

[25] Yuan, T., Y. Cheng, H. Wang, and Y. Qin, "Beam steering for electromagnetic vortex imaging using uniform circular arrays," *IEEE Antennas and Wireless Propagation Letters*, Vol. 16, 704–707, 2016.

[26] Wang, Y.-W., G.-M. Wang, and B.-F. Zong, "Directivity improvement of Vivaldi antenna using double-slot structure," *IEEE Antennas and Wireless Propagation Letters*, Vol. 12, 1380–1383, 2013.

[27] Liu, B., Y. Cui, and R. Li, "A broadband dual-polarized dual-OAM-mode antenna array for OAM communication," *IEEE Antennas and Wireless Propagation Letters*, Vol. 16, 744–747, 2016.

[28] Xiao, Z., J. Lei, J. Lin, and W. Li, "Ultra-wideband vortex wave array based on vivaldi antenna elements," in *2023 International Applied Computational Electromagnetics Society Symposium (ACES-China)*, 1–3, 2023.

[29] Yang, T., D. Yang, B. Wang, and J. Hu, "Experimentally validated, wideband, compact, OAM antennas based on circular Vivaldi antenna array," *Progress In Electromagnetics Research C*, Vol. 80, 211–219, Jan. 2018.

[30] Deng, C., W. Chen, Z. Zhang, Y. Li, and Z. Feng, "Generation of OAM radio waves using circular Vivaldi antenna array," *International Journal of Antennas and Propagation*, Vol. 2013, Mar. 2013.